

Numerical Computation of Two-loop Box Diagrams with Masses

F. Yuasa^{a,*}, E. de Doncker^b, N. Hamaguchi^a, T. Ishikawa^a, K. Kato^c, Y. Kurihara^a, J. Fujimoto^a, Y. Shimizu^a

^aHigh Energy Accelerator Research Organization (KEK), 1-1 Oho Tsukuba, Ibaraki 305-0801, Japan

^bWestern Michigan University Kalamazoo, MI 49008-5371, USA

^cKogakuin University, 1-24 Nishi-Shinjuku, Shinjuku, Tokyo 163-8677, Japan

Abstract

A new approach is presented to evaluate multi-loop integrals, which appear in the calculation of cross-sections in high-energy physics. It relies on a fully numerical method and is applicable to a wide class of integrals with various mass configurations. As an example, the computation of two-loop planar and non-planar box diagrams is shown. The results are confirmed by comparisons with other techniques, including the reduction method, and by a consistency check using the dispersion relation.

Keywords: multi-loop integrals, electroweak interaction, numerical integration, extrapolation method

PACS: 12.15.Lk, 02.60.Jh

1. Introduction

In the study of high-energy reactions observed at current and future accelerators, such as LHC and ILC, precise theoretical predictions of cross-sections including higher order corrections are required. This is due to the fact that the lowest order approximation in perturbative calculations of quantum field theory is not sufficiently accurate to be compared to the experimental data. One has to take into account the contributions from higher order terms as well. In order to include these corrections in the Standard model or beyond, it is indispensable to handle the evaluation of loop integrals.

At the one-loop level it is known that analytic solutions exist for any type of diagram, and the results are expressed in terms of known functions, such as logarithms and Spence functions (see, for example [1]). Using these analytic results several automatic computation systems [2, 3, 4, 5, 6, 7, 8, 9, 10] have been proposed. In order to estimate cross sections we need automatic computation systems because we may have to deal with a large number of relevant Feynman diagrams for a given process.

However, the extension of the system to include higher order corrections is not an easy task, because analytic integration is generally impossible for higher loop diagrams, especially for diagrams which depend on more general mass configurations. Analytic results are only known for a limited class of two-loop diagrams. Therefore we have to rely on numerical evaluations. We need to establish efficient methods that can be incorporated into automatic computation systems of cross-sections. For a number of years we have gained experience evaluating one-loop integrals numerically, where the results can be compared with known analytic answers. We succeeded in calculating vertex, box and pentagon diagrams with arbitrary masses [11, 12, 13, 14, 15, 16, 17, 18, 19, 20, 21, 22]. We also computed two-loop self-energy and vertex diagrams. Further related work can be found in [23, 24, 25, 26, 27, 28, 29, 30, 31, 32, 33, 34, 35, 36, 37, 38, 39].

In our method we start from the Feynman parameter representation of loop integrals. We employ a fully numerical integration procedure combined with numerical extrapolation. The purpose of this paper is to describe the method in detail and to show results for more complicated loop integrals, corresponding to two-loop box diagrams with massive

*Corresponding author.

E-mail address: fukuko.yuasa@kek.jp (F.Yuasa), Tel: +81-29-879-6009, Fax: +81-29-864-4402, Postal address: 1-1 Oho Tsukuba Ibaraki 305-0801 Japan.

particles. For simplicity we deal with scalar loop integrals throughout this paper, ignoring all spin complications that are irrelevant to the essential discussion of the numerical approach.

The most general form of the scalar integral for a diagram with L loops and N internal lines is given by

$$\mathcal{I} = \prod_{j=1}^L \int \frac{d^n l_j}{i(2\pi)^n} \prod_{r=1}^N \frac{1}{D_r} \quad (1)$$

where l_j is the j -th loop momentum in the n -dimensional space-time, and

$$D_r = q_r^2 - m_r^2 + i\epsilon \quad (2)$$

is the inverse of the r -th Feynman propagator, where ϵ denotes an infinitesimal quantity, m_r is the mass of the r -th particle, and the momentum q_r flowing on the r -th internal line is given by a sum of loop and external momenta. We make use of the Feynman identity,

$$\prod_{r=1}^N \frac{1}{D_r} = \Gamma(N) \int_0^1 \prod_{r=1}^N dx_r \frac{\delta(1 - \sum x_r)}{(\sum x_r D_r)^N}. \quad (3)$$

Carrying out the loop momentum integrations delivers

$$\mathcal{I} = \left(\frac{1}{4\pi}\right)^{nL/2} \Gamma\left(N - \frac{nL}{2}\right) \times I, \quad (4)$$

where

$$I = (-1)^N \int_0^1 \prod_{i=1}^N dx_i \delta(1 - \sum x_i) \frac{C^{N-n(L+1)/2}}{(D - i\epsilon C)^{N-nL/2}}. \quad (5)$$

The function D is a polynomial in the Feynman parameters $\{x_i\}$. D further involves physical variables such as the external momenta and particle masses. The function C is also a polynomial in the $\{x_i\}$. Both functions are determined by the topology of the Feynman diagram. Details of their construction are summarized in Appendix A.

In the two-loop box diagrams, D depends on two kinematical variables s and t , where s is the square of the total energy of the colliding particle system, and $t < 0$ is the squared momentum transfer between the initial and the final particles. For the infrared divergent integrals, we have two prescriptions. One is to introduce a small fictitious mass λ for the massless particles and the other is the dimensional regularization technique. In the former we can set $n = 4$ in Eq.(5) and the procedure is straightforward once the value λ is fixed [14, 16]. For the latter we put $n = 4 + 2\delta = n(\delta)$ and use a *double extrapolation technique* for both ϵ and δ (from $n(\delta)$) in Eq.(5) [20, 21]. Here we estimate the integral for a fixed value of δ using the extrapolation with respect to ϵ . Repeating this for a series of δ values, we can estimate the pole residue of $1/\delta$ and the finite part of the integral numerically.

We briefly describe the general properties of the integral I and give some terminology. Depending on the value of s , the function D in the denominator may vanish in the integration domain. In this case, the infinitesimal parameter ϵ prevents I from diverging. Then I exhibits an imaginary part even if all the physical parameters s , t and the masses are real. This region of s is called the *physical region*, where s exceeds the threshold energy, so that the reaction takes place. On the other hand, in the *unphysical region*, s is lower than the threshold. This is the region of s where we can put $\epsilon = 0$ and the integral is real for real s . Thus the integral I can be regarded as an analytic function in the complex s -plane with cuts along the real s -axis, starting at branch points which are determined by physics conditions. However, as we shall see below in Section 3, we treat ϵ not as infinitesimal but as a *finite* number in the numerical procedure for calculating $\Re(I)$ and $\Im(I)$, $I = \Re(I) + i\Im(I)$, in the physical region.

This paper is outlined as follows. In Section 2 we construct the integrands for two-loop box diagrams ($L = 2$ and $N = 7$), and present suitable variable transformations. We explain the details of our techniques in Section 3; and the results of the computations are shown in Section 4. Section 5 is devoted to a discussion on how to assess the correctness of the obtained results. Section 6 gives conclusions and future directions for this work.

2. Two-loop box integrals

The topology of the two-loop box diagram is depicted in Fig. 1. We call Fig. 1(a) the planar diagram and Fig. 1(b) the non-planar diagram, respectively. The loop integral in the Feynman parameters (x_1, \dots, x_7) is of the form

$$I = - \int_0^1 dx_1 dx_2 dx_3 dx_4 dx_5 dx_6 dx_7 \delta(1 - \sum_{\ell=1}^7 x_\ell) \frac{C}{(D - i\epsilon C)^3}. \quad (6)$$

Here, D and C are polynomials of Feynman parameters. Their derivations are given in Appendix A.

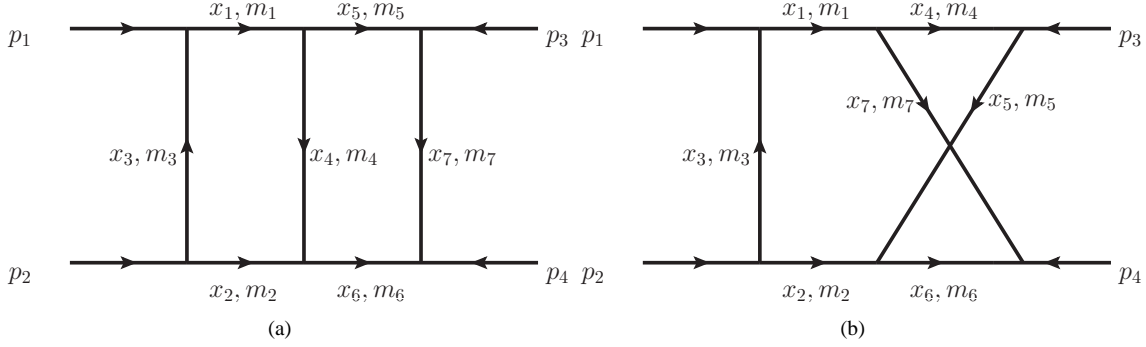


Figure 1: (a) Two-loop planar box diagram (b) Two-loop non-planar box diagram

The external momenta p_1, p_2, p_3 and p_4 are defined to flow inward, satisfying $p_1 + p_2 + p_3 + p_4 = 0$. The kinematical variables s and t are given by

$$\begin{aligned} s &= (p_1 + p_2)^2 = (p_3 + p_4)^2, \\ t &= (p_1 + p_3)^2 = (p_2 + p_4)^2. \end{aligned}$$

For later notational convenience we introduce a third kinematical variable u by

$$u = (p_1 + p_4)^2 = (p_2 + p_3)^2.$$

The variables s, t and u are not independent, as

$$s + t + u = p_1^2 + p_2^2 + p_3^2 + p_4^2.$$

In the following we derive the explicit formulae of the functions D and C . We also show examples of variable transformations, which allow eliminating a common factor in the numerator and denominator. Furthermore, the resulting form of the integral will be suited for an application of the reduction formalism given in Section 5.1. Followed by a Monte Carlo integration we will use the latter for the purpose of comparing of its numerical results with those by DCM.

2.1. Explicit formulae of the functions D and C for the planar diagram

The functions D and C in Eq. (6), corresponding to Fig. 1(a), are given by

$$\begin{aligned} D &= C \sum_{\ell} x_\ell m_\ell^2 \\ &- \{s(x_1 x_2 (x_4 + x_5 + x_6 + x_7) + x_5 x_6 (x_1 + x_2 + x_3 + x_4) + x_1 x_4 x_6 + x_2 x_4 x_5) \\ &+ t x_3 x_4 x_7 \\ &+ p_1^2 (x_3 (x_1 x_4 + x_1 x_5 + x_1 x_6 + x_1 x_7 + x_4 x_5)) \\ &+ p_2^2 (x_3 (x_2 x_4 + x_2 x_5 + x_2 x_6 + x_2 x_7 + x_4 x_6)) \\ &+ p_3^2 (x_7 (x_1 x_4 + x_1 x_5 + x_2 x_5 + x_3 x_5 + x_4 x_5)) \\ &+ p_4^2 (x_7 (x_1 x_6 + x_2 x_4 + x_2 x_6 + x_3 x_6 + x_4 x_6))\}, \end{aligned} \quad (7)$$

and

$$C = (x_1 + x_2 + x_3 + x_4)(x_4 + x_5 + x_6 + x_7) - x_4^2. \quad (8)$$

Using the transformation $(x_1, x_2, x_3, x_4, x_5, x_6, x_7) \rightarrow (\rho_1, \rho_2, \rho_3, u_1, u_2, u_3, u_4)$, defined by $x_1 = \rho_1 u_1$, $x_2 = \rho_1 u_2$, $x_3 = \rho_1(1 - u_1 - u_2)$, $x_4 = \rho_3$, $x_5 = \rho_2 u_3$, $x_6 = \rho_2 u_4$ and $x_7 = \rho_2(1 - u_3 - u_4)$, we obtain

$$\int dx_1 \cdots dx_7 \delta(1 - \sum x_j) = \int d\rho_1 d\rho_2 d\rho_3 \delta(1 - \sum \rho_j) \rho_1^2 \rho_2^2 \int du_1 du_2 du_3 du_4,$$

with

$$\rho_1 + \rho_2 + \rho_3 = 1, \quad 0 \leq u_1 + u_2 \leq 1, \quad 0 \leq u_3 + u_4 \leq 1,$$

and with Jacobian $\rho_1^2 \rho_2^2$. Changing the variables by $\rho_1 = \rho\xi$, $\rho_2 = \rho(1 - \xi)$ and $\rho_3 = 1 - \rho$ gives

$$\int d\rho_1 d\rho_2 d\rho_3 \delta(1 - \sum \rho_j) \rho_1^2 \rho_2^2 \cdots = \int_0^1 d\rho \int_0^1 d\xi \rho^5 \xi^2 (1 - \xi)^2 \cdots$$

After these transformations, D and C contain a common factor ρ and we set $\mathcal{D} = D/\rho$ and $\mathcal{C} = C/\rho$. The integral becomes

$$I_{planar} = - \int_0^1 d\rho \int_0^1 d\xi \int_0^1 du_1 \int_0^{1-u_1} du_2 \int_0^1 du_3 \int_0^{1-u_3} du_4 \frac{\mathcal{C}}{(\mathcal{D} - i\epsilon\mathcal{C})^3} \rho^3 \xi^2 (1 - \xi)^2, \quad (9)$$

where \mathcal{D} is a quadratic in $\mathbf{u} = (u_1, u_2, u_3, u_4)^T$,

$$\mathcal{D} = \mathbf{u}^T A \mathbf{u} + \mathbf{B}^T \mathbf{u} + c, \quad (10)$$

and

$$\mathcal{C} = \rho\xi(1 - \xi) + 1 - \rho. \quad (11)$$

The 4×4 matrix A is symmetric and depends on the internal masses m_ℓ ($1 \leq \ell \leq 7$), and on the kinematical variables, s and t . In this paper we assume $p_1^2 = p_2^2 = p_3^2 = p_4^2 = m^2$ for both diagrams. When $m_1 = m_2 = m_5 = m_6 = m$ and $m_3 = m_4 = m_7 = M$ ($m \neq M$), we have

$$A = \begin{pmatrix} \rho\xi^2(1 - \rho\xi)A_1 & \rho\xi(1 - \rho)(1 - \xi)A_2 \\ \rho\xi(1 - \rho)(1 - \xi)A_2 & \rho(1 - \xi)^2(1 - \rho(1 - \xi))A_1 \end{pmatrix},$$

where the 2×2 matrices A_1 and A_2 are

$$A_1 = \begin{pmatrix} -m^2 & s/2 - m^2 \\ s/2 - m^2 & -m^2 \end{pmatrix}, \quad A_2 = \begin{pmatrix} t/2 - m^2 & s/2 + t/2 - m^2 \\ s/2 + t/2 - m^2 & t/2 - m^2 \end{pmatrix}.$$

The vector \mathbf{B} is given by

$$\mathbf{B} = \begin{pmatrix} -t\rho\xi(1 - \rho)(1 - \xi) + M^2\rho\xi\mathcal{C} \\ -t\rho\xi(1 - \rho)(1 - \xi) + M^2\rho\xi\mathcal{C} \\ -t\rho\xi(1 - \rho)(1 - \xi) + M^2\rho(1 - \xi)\mathcal{C} \\ -t\rho\xi(1 - \rho)(1 - \xi) + M^2\rho(1 - \xi)\mathcal{C} \end{pmatrix},$$

and the scalar c is

$$c = t\rho\xi(1 - \rho)(1 - \xi) - M^2\mathcal{C}.$$

The quadratic form will further be used in Section 5.1 for a comparison of DCM with a reduction method.

2.2. Explicit formulae of the functions D and C for the non-planar diagram

The functions D and C in Eq. (6), corresponding to Fig. 1(b), are

$$\begin{aligned}
D &= C \sum_{\ell} x_{\ell} m_{\ell}^2 \\
&- \{s(x_1 x_2 x_4 + x_1 x_2 x_5 + x_1 x_2 x_6 + x_1 x_2 x_7 + x_1 x_5 x_6 + x_2 x_4 x_7 - x_3 x_4 x_6) \\
&+ t(x_3(-x_4 x_6 + x_5 x_7)) \\
&+ p_1^2(x_3(x_1 x_4 + x_1 x_5 + x_1 x_6 + x_1 x_7 + x_4 x_6 + x_4 x_7)) \\
&+ p_2^2(x_3(x_2 x_4 + x_2 x_5 + x_2 x_6 + x_2 x_7 + x_4 x_6 + x_5 x_6)) \\
&+ p_3^2(x_1 x_4 x_5 + x_1 x_5 x_7 + x_2 x_4 x_5 + x_2 x_4 x_6 + x_3 x_4 x_5 + x_3 x_4 x_6 + x_4 x_5 x_6 + x_4 x_5 x_7) \\
&+ p_4^2(x_1 x_4 x_6 + x_1 x_6 x_7 + x_2 x_5 x_7 + x_2 x_6 x_7 + x_3 x_4 x_6 + x_3 x_6 x_7 + x_4 x_6 x_7 + x_5 x_6 x_7)\}
\end{aligned} \tag{12}$$

and

$$C = (x_1 + x_2 + x_3 + x_4 + x_5)(x_1 + x_2 + x_3 + x_6 + x_7) - (x_1 + x_2 + x_3)^2. \tag{13}$$

The transformation $(x_1, x_2, x_3, x_4, x_5, x_6, x_7) \rightarrow (\rho_1, \rho_2, \rho_3, u_1, u_2, u_3, u_4)$, defined by $x_1 = \rho_1 u_1$, $x_2 = \rho_1 u_2$, $x_3 = \rho_1(1 - u_1 - u_2)$, $x_4 = \rho_2 u_3$, $x_5 = \rho_2(1 - u_3)$, $x_6 = \rho_3 u_4$ and $x_7 = \rho_3(1 - u_4)$, yields

$$\int dx_1 \cdots dx_7 \delta(1 - \sum x_j) = \int d\rho_1 d\rho_2 d\rho_3 \delta(1 - \sum \rho_j) \rho_1^2 \rho_2 \rho_3 \int du_1 du_2 du_3 du_4,$$

with

$$\rho_1 + \rho_2 + \rho_3 = 1, \quad 0 \leq u_1 + u_2 \leq 1, \quad 0 \leq u_3 \leq 1, \quad 0 \leq u_4 \leq 1,$$

and the Jacobian is $\rho_1^2 \rho_2 \rho_3$. The change of variables $\rho_1 = 1 - \rho$, $\rho_2 = \rho \xi$ and $\rho_3 = \rho(1 - \xi)$ gives

$$\int d\rho_1 d\rho_2 d\rho_3 \delta(1 - \sum \rho_j) \rho_1^2 \rho_2 \rho_3 \cdots = \int_0^1 d\rho \int_0^1 d\xi \rho^3 (1 - \rho)^2 \xi (1 - \xi) \cdots,$$

with

$$0 \leq \rho \leq 1, \quad 0 \leq \xi \leq 1.$$

Similar to the case of the planar diagram, D and C contain a common factor ρ . Putting $\mathcal{D} = D/\rho$ and $\mathcal{C} = C/\rho$, delivers the final form of the integral

$$I_{non-planar} = - \int_0^1 d\rho \int_0^1 d\xi \int_0^1 du_1 \int_0^{1-u_1} du_2 \int_0^1 du_3 \int_0^1 du_4 \frac{\mathcal{C}}{(\mathcal{D} - i\epsilon\mathcal{C})^3} \rho(1 - \rho)^2 \xi(1 - \xi), \tag{14}$$

where \mathcal{D} is a quadratic in $\mathbf{u} = (u_1, u_2, u_3, u_4)^T$, given by

$$\mathcal{D} = \mathbf{u}^T A \mathbf{u} + \mathbf{B}^T \mathbf{u} + c, \tag{15}$$

and

$$\mathcal{C} = \rho \xi (1 - \xi) + 1 - \rho. \tag{16}$$

With the mass assignment as $m_1 = m_2 = m_4 = m_6 = m$ and $m_3 = m_5 = m_7 = M$ ($m \neq M$) we have

$$A = \begin{pmatrix} (1 - \rho)^2 A_1 & \rho \xi (1 - \rho)(1 - \xi) A_2 \\ \rho \xi (1 - \rho)(1 - \xi) A_2 & A_3 \end{pmatrix},$$

where the 2×2 matrices A_1 , A_2 and A_3 are

$$A_1 = \begin{pmatrix} -m^2 & s/2 - m^2 \\ s/2 - m^2 & -m^2 \end{pmatrix}, \quad A_2 = \begin{pmatrix} t/2 - m^2 & s/2 + t/2 - m^2 \\ s/2 + t/2 - m^2 & t/2 - m^2 \end{pmatrix},$$

$$A_3 = \begin{pmatrix} -m^2\rho\xi^2(1-\rho\xi) & (-s/2+m^2)\rho(1-\rho)\xi(1-\xi) \\ (-s/2+m^2)\rho(1-\rho)\xi(1-\xi) & -m^2\rho(1-\xi)^2(1-\rho(1-\xi)) \end{pmatrix}.$$

The vector \mathbf{B} is given by

$$\mathbf{B} = \begin{pmatrix} -t\rho\xi(1-\rho)(1-\xi) + M^2(1-\rho)\mathcal{C} \\ -t\rho\xi(1-\rho)(1-\xi) + M^2(1-\rho)\mathcal{C} \\ -t\rho\xi(1-\rho)(1-\xi) + M^2\rho\xi\mathcal{C} \\ -t\rho\xi(1-\rho)(1-\xi) + M^2\rho(1-\xi)\mathcal{C} \end{pmatrix},$$

and the scalar c is

$$c = t\rho(1-\rho)\xi(1-\xi) - M^2\mathcal{C}.$$

Note the similarity between the Eqs. (9) and (14) of the planar and the non-planar integral, respectively, obtained via the transformations in Sections 2.1 and 2.2. The transformed integrand functions (of both 6-dimensional integrals) involve a function \mathcal{D} in the denominator, which is a quadratic in the variables u_1, u_2, u_3 and u_4 . This form of the integrand will further lend itself to the reduction method of Section 5.1 (which will be used for a comparison of the numerical results). As an aside, the form of the 4-dimensional integral in u_1, u_2, u_3, u_4 also resembles that of the one-loop pentagon integral, e.g., in [19].

3. Numerical techniques

We introduce the *Direct Computation Method* (DCM), based on a combination of numerical integration, and extrapolation on a sequence of integrals. DCM comprises the following three steps:

1. Let ϵ in Eq. (5) be a finite value determined by a (scaled) geometric sequence

$$\epsilon = \epsilon_l = \epsilon_0 / (A_c)^l, l = 0, 1, \dots, \quad (17)$$

for a constant ϵ_0 and base $0 < 1/A_c < 1$.

2. Evaluate the multi-dimensional integral I of Eq. (5) numerically. In view of the finite ϵ_l we obtain a finite value for the integral corresponding to each l . Thus a sequence of $I(\epsilon_l)$, $l = 0, 1, 2, \dots$ is generated.
3. Extrapolate the sequence $I(\epsilon_l)$ to the limit as $\epsilon_l \rightarrow 0$ with the purpose of calculating I as $\lim_{\epsilon \rightarrow 0} I(\epsilon)$.

If D does not vanish within the integration region, we can ignore ϵ and no extrapolation is needed as $I = I(\epsilon) |_{\epsilon=0}$.

For multi-dimensional integration we make use of the DQAGE routine in the QUADPACK [40] package. DQAGE uses a variant of Gaussian quadrature, where the sampling points are given by a Gauss-Kronrod rule pair in each subinterval. The Gauss rule with ν points has polynomial degree of accuracy $d_\nu = 2\nu - 1$; i.e., it is exact for polynomials of degree $d = 0, \dots, d_\nu$ and not for all polynomials of degree $d_\nu + 1$. The corresponding Kronrod rule re-uses the abscissas of the Gauss rule and adds $\nu + 1$ points interlacing with those of the Gauss rule. The Kronrod rule with $2\nu + 1$ points has polynomial degree $3\nu + 1$ if this number is odd (for ν even), and otherwise $3\nu + 2$ (for ν odd).

On input for DQAGE, the user selects one of six Gauss-Kronrod pairs, with 15, 21, 31, 41, 51 or 61 points, via the input parameter `key = 1, 2, 3, 4, 5, or 6`, respectively. The rule pair produces the Kronrod rule value as the integral approximation, together with an estimate of the absolute error on each subinterval (which is based on the difference between the Gauss and the Kronrod result on the subinterval). This allows the selection of that subinterval with the largest estimated error, as the next interval to be subdivided in successive steps of the adaptive partitioning strategy of DQAGE. The user imposes a bound on the number of subdivisions via the input parameter `limit`. As a result of the adaptive partitioning, the algorithm subdivides intensively around singularities, so that hot spots emerge where singularities or other irregular integrand behavior occur within the integration interval. For multi-dimensional integration we apply DQAGE in a repeated (iterated) quadrature for successive coordinate directions [41].

In DCM, the accuracy of the result depends on that of the calculated sequence of integrals $I(\epsilon_l)$, $l = 0, 1, \dots$. Since the integration error affects the accuracy of the extrapolation, we want to compute the integrals $I(\epsilon_l)$ to at least an order of magnitude more accuracy than that expected for the final result. On the other hand, the CPU time is

directly related to the accuracy requirement. Thus, adequate values need to be specified for the input parameters `key` and `limit` of the DQAGE routine in each dimension, to control the overall work and the termination of the algorithm. For the computation of two-loop box integrals, we find that `key` = 1 or 2 and `limit` = 10 ~ 30 are suitable values.

We use Wynn's ε -algorithm[42, 43] for the extrapolation, which works efficiently under fairly general conditions, even for very slowly convergent sequences or series. The ε algorithm is applied to the sequence $I(\epsilon_l), l = 0, 1, \dots$ obtained by multi-dimensional integration. We define the table elements $a(l, k)$ of the extrapolation table with initial values

$$a(l, -1) = 0, \quad a(l, 0) = I(\epsilon_l), \quad l = 0, 1, \dots \quad (18)$$

The element $a(l, k + 1)$ is obtained from $a(l, k)$ and $a(l, k - 1)$ by the following recurrence relation:

$$a(l, k + 1) = a(l + 1, k - 1) + \frac{1}{a(l + 1, k) - a(l, k)}, \quad l = 0, 1, \dots \quad (19)$$

Whilst the $a(l, k)$'s with odd k are meant to store temporary numbers, the $a(l, k)$'s with even k give extrapolated estimates.

We use the ε -algorithm code from the QUADPACK [40] package. With each new $I(\epsilon_l)$, a new lower diagonal can be added to the extrapolation table. At each iteration only the last two lower diagonals need to be stored for this computation. Along with each new table element $a(m, n)$ where n is even, an error estimate is calculated based on differences with its neighboring elements. In a converging table, the even-numbered columns as well as the diagonals converge to the limit $\lim_{\epsilon \rightarrow 0} I(\epsilon) = I$ (barring roundoff). Among the even-column indexed table elements along newly computed lower diagonal, the ε -algorithm code selects the "best" $a(m, n)$ (with the least error estimate). The CPU time for the extrapolation is negligible compared to that of the integration.

We further have to use some heuristics for the computation of the extrapolated sequence. The acceleration constant A_c in (17) can usually be set to 2. In cases where the integration is very difficult for decreasing ϵ_l , a smaller value of A_c is used, e.g., $A_c = 1.3$ or 1.2 , yielding a sequence of $\epsilon_l, l = 0, 1, \dots$ which decreases more slowly. To determine the initial value of the geometric sequence, we assign ϵ_0 depending on the squared mass appearing in function D . We parametrize ϵ_0 in the form $\epsilon_0 = A_c^\gamma$, where the parameter γ can be adjusted. The choice of these parameters influence the accuracy of the result.

For the two-loop box integral computations reported in the next section, we found $A_c = 1.2$ and γ around 40 to be adequate values. The accuracy achieved is restricted by the actual CPU time needed. If the computation time is excessive, we have to accept less accurate results. This happens, for example, when s is much greater than $10m^2$. Thus the accuracy is different from point to point in the plots shown below. All the computations are done in double precision arithmetic.

4. Numerical results

According to the prescription of DCM in the previous section, we evaluate both I_{planar} and $I_{\text{non-planar}}$ given by Eqs. (9) and (14), respectively. In both cases the kinematical variable s is varied but t is fixed at $t = -10000\text{GeV}^2$ throughout the computations. We introduce the dimensionless variable

$$f_s = \frac{s}{m^2}. \quad (20)$$

For the mass parameters we set $m = 50 \text{ GeV}$ and $M = 90 \text{ GeV}$.

4.1. Planar diagram

In previous work [19] we presented results of the real part integral in the physical region, $4.5 \leq f_s \leq 25.0$. Here we evaluate the integral in the region $0.0 \leq f_s \leq 25.0$ for the real part and the imaginary part. The results are depicted in Fig. 2 where the data points represent the integral values and the lines merely connect the points as a guide for the eyes. The s -channel threshold starts at $f_s = 4.0$ corresponding to $s = 4m^2$. For example, we set $\epsilon_0 = 1.2^{45}$, `key` = 1 and `limit` = 10 in all dimensions for the real part at $f_s = 10.0$ and it took 8.5 days to obtain the result with enough accuracy as 0.01% using a system with Intel Xeon CPU E5430 @ 2.66GHz.

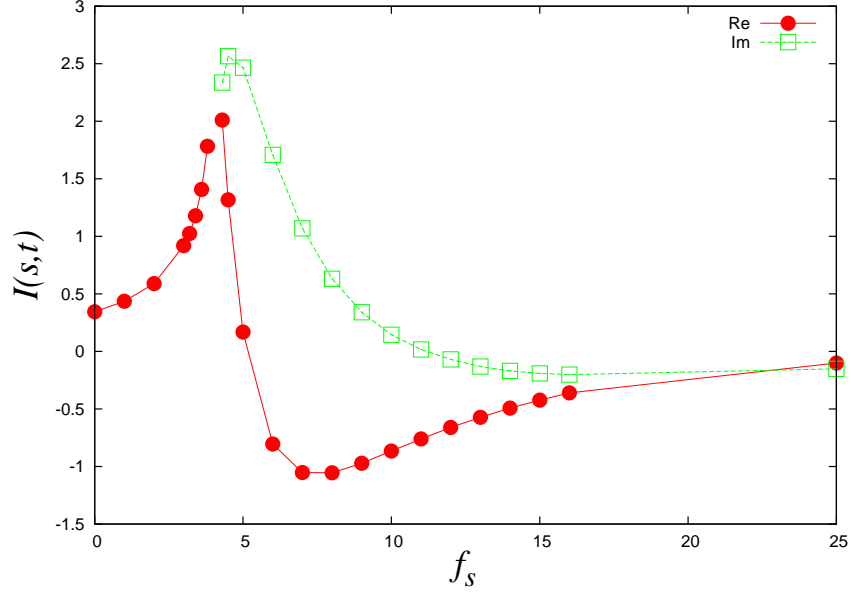


Figure 2: Numerical results of $\Re(I_{planar})$ and $\Im(I_{planar})$ in units of $10^{-12} \text{ GeV}^{-6}$ for $0.0 \leq f_s \leq 25.0$ and $t = -10000.0 \text{ GeV}^2$. Plotted points are the real part (bullets) and the imaginary part (squares).

4.2. Non-planar diagram

Fig. 3 shows the results for $-20.0 \leq f_s \leq 20.0$. Different from the planar case, it is known that $I_{non-planar}$ has two cuts; one starts from the normal s -channel threshold, $s = 4m^2$, and the other from $s = -t - M^2 - 4mM$ to $s = -\infty$. The latter corresponds to the u -channel threshold at $u = (M + 2m)^2$. These correspond to $f_s = 4.0$ and $f_s = -6.44$, respectively. In Fig. 3 we also show some results of the imaginary part in the range $-100.0 \leq f_s \leq -20.0$. In this region the imaginary part is small but its contribution is not negligible when it is put in the dispersion integral (32) of Section 5.2.

In the physical region the computation time tends to be longer for larger f_s . This applies to both the planar and the non-planar diagram. For example the time required to obtain the real part of the non-planar box integral with enough accuracy as 0.003% at $f_s = 10.0$ (with $\epsilon_0 = 1.2^{40}$, `key` = 2 in all dimensions, and `limit` = 10, 20, 20, 10, 10, 10 in consecutive dimensions) is about a week using a system with Intel Xeon CPU X5365 @ 3.16GHz. For much greater f_s it may become more difficult to get an answer in a practical time. However, this computation time is measured using a single CPU. It can potentially be shortened by applying parallel computing techniques on (possibly distributed) multi-core processors [17, 44, 45].

5. Validation of the results

After obtaining answers by the numerical computation, the most important issue is how to confirm that the results are correct and reliable. It would be most desirable to have answers available by independent methods. For example, we computed the result $0.10364072096 \pm (0.315 \times 10^{-7})$ for the planar integral, with $s = t = 1 \text{ GeV}^2$ and $m_i^2 = 1 \text{ GeV}^2$ ($1 \leq i \leq 7$), $p_i^2 = 1 \text{ GeV}^2$ ($1 \leq i \leq 4$). We were able to compare this to the value 0.1036407209893 evaluated by the program SYS [46] and found good agreement. With the same values of the kinematical variables we obtained the non-planar integral as $0.08535139 \pm (0.105 \times 10^{-7})$, but no result was available by SYS. This comparison demonstrates that the expressions of the functions C and D for the planar diagram are correct and that DQAGE works as expected. In these examples, D does not vanish within the integration region; thus we do not need extrapolation. The CPU time required for both the planar and the non-planar diagram is less than 2 min. using a Xeon CPU X5365 @ 3.16GHz.

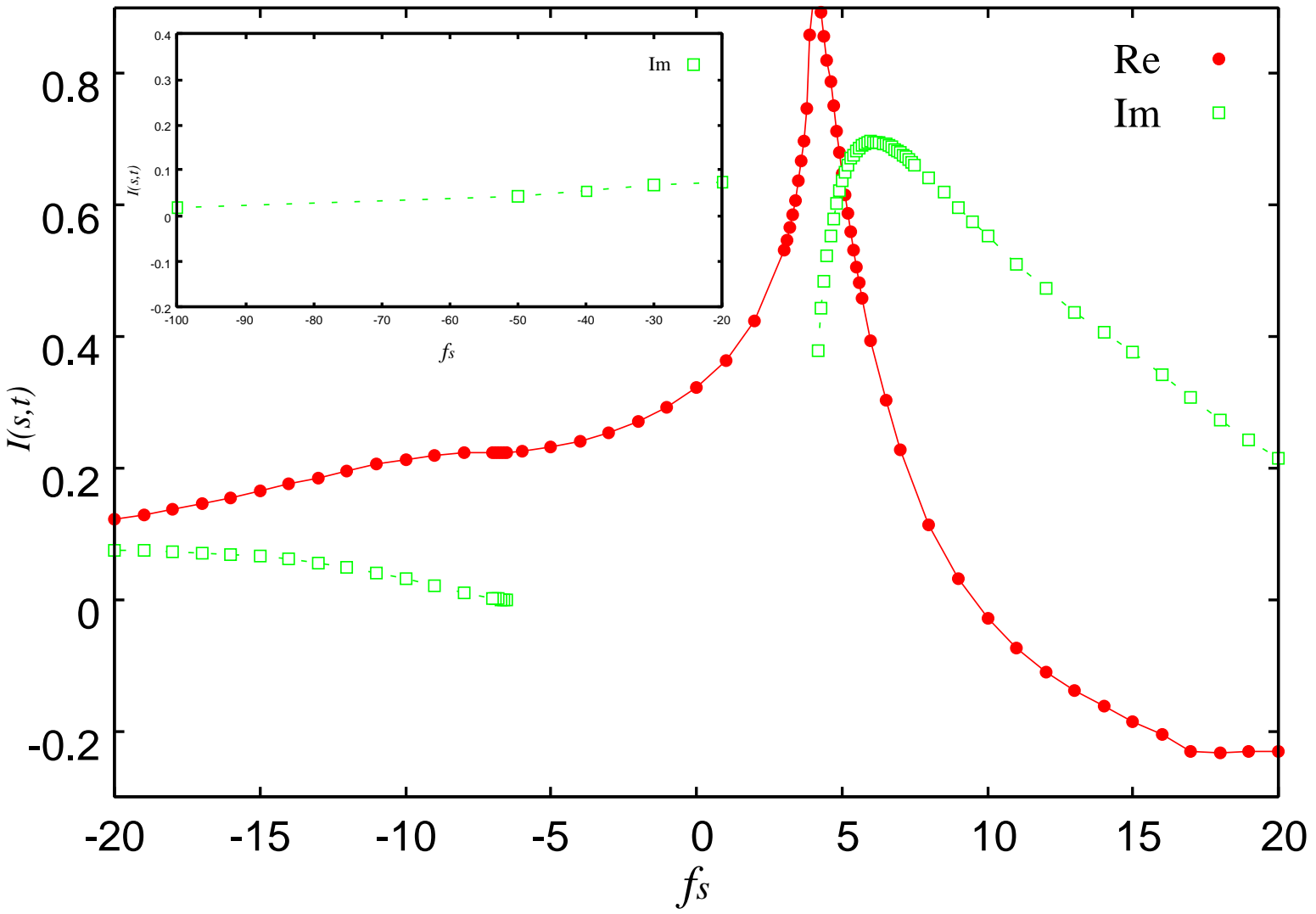


Figure 3: Numerical results of $\Re(I_{non-planar})$ and $\Im(I_{non-planar})$ for $-20.0 \leq f_s \leq 20.0$ and of $\Im(I_{non-planar})$ for $-100.0 \leq f_s \leq -20.0$ with $t = -10000.0 \text{ GeV}^2$ in units of $10^{-12} \text{ GeV}^{-6}$. Plotted points are the real part (bullets) and the imaginary part (squares).

Below we outline an integration method based on reduction formulas, and explain how to use it for a consistency check.

5.1. Comparison with the reduction method

Consider a quadratic form \mathcal{D} in N variables, $\mathbf{u} = (u_1, \dots, u_N)$,

$$\mathcal{D} = \mathbf{u}^T A \mathbf{u} + \mathbf{B}^T \mathbf{u} + c, \quad (21)$$

where A is an N -dimensional symmetric matrix $A = (A_{ij})$, \mathbf{B} is an N -dimensional vector $\mathbf{B}^T = (B_1, \dots, B_N)$, with constant coefficients. Here c contains not only a real part but also $-i\epsilon\mathcal{C}$ with an infinitesimal ϵ . Assuming A is invertible, we define the vector

$$\mathbf{X}^T = 2\mathbf{u}^T + \mathbf{B}^T A^{-1}. \quad (22)$$

Then we have

$$\mathbf{X}^T (\nabla \mathcal{D}) = 4(\mathcal{D} - c) + \mathbf{B}^T A^{-1} \mathbf{B} = 4\mathcal{D} + \Delta_N, \quad (23)$$

with $\nabla^T = (\partial/\partial u_1, \dots, \partial/\partial u_N)$. Here Δ_N is defined as

$$\Delta_N = \mathbf{B}^T A^{-1} \mathbf{B} - 4c. \quad (24)$$

We divide Eq. (23) by $\mathcal{D}^{\alpha+1}$ where $\alpha \geq 0$ is an arbitrary number. Using the relation

$$\nabla^T \left(\frac{\mathbf{X}}{\mathcal{D}^\alpha} \right) = \frac{2N}{\mathcal{D}^\alpha} - \alpha \frac{\mathbf{X}^T \nabla \mathcal{D}}{\mathcal{D}^{\alpha+1}} \quad (25)$$

we obtain the following reduction formula

$$\frac{\Delta_N}{\mathcal{D}^{\alpha+1}} = \frac{-4 + 2N/\alpha}{\mathcal{D}^\alpha} - \frac{1}{\alpha} \nabla^T \left(\frac{\mathbf{X}}{\mathcal{D}^\alpha} \right), \quad \text{for } \alpha > 0. \quad (26)$$

It should be noted that the power of the denominator in the right-hand side is decreased by one, compared to the left-hand side, that is, the singular behavior is softened. When $\alpha = 0$ we find

$$\frac{\Delta_N}{\mathcal{D}} = -4 - 2N \log \mathcal{D} + \nabla^T (\mathbf{X} \log \mathcal{D}). \quad (27)$$

When a polynomial in \mathbf{u} , $f(\mathbf{u}) \neq 1$, occurs in the numerator of the left-hand side, the formulas are generalized to

$$\frac{f \Delta_N}{\mathcal{D}^{\alpha+1}} = \frac{-4f + \nabla^T (f \mathbf{X})/\alpha}{\mathcal{D}^\alpha} - \frac{1}{\alpha} \nabla^T \left(\frac{f \mathbf{X}}{\mathcal{D}^\alpha} \right), \quad \text{for } \alpha > 0 \quad (28)$$

and

$$\frac{f \Delta_N}{\mathcal{D}} = -4f - \nabla^T (f \mathbf{X}) \log \mathcal{D} + \nabla^T (f \mathbf{X} \log \mathcal{D}). \quad (29)$$

We apply the formula to the functions \mathcal{D} given in Eqs. (10) and (15), which are quadratics in u_1, \dots, u_4 . Since we have $N = 2\alpha$ ($N = 4, \alpha = 2$) in both cases, we find a simpler formula

$$\frac{\Delta_4}{\mathcal{D}^3} = -\frac{1}{2} \nabla^T \left(\frac{\mathbf{X}}{\mathcal{D}^2} \right), \quad (30)$$

with $\Delta_4 = \Delta_4(\rho, \xi)$. By integrating we have

$$\int d(\mathbf{u}) \frac{1}{\mathcal{D}^3} = -\frac{1}{2\Delta_4} \int d(\mathbf{u}) \nabla^T \left(\frac{\mathbf{X}}{\mathcal{D}^2} \right), \quad d(\mathbf{u}) = \prod_{j=1}^4 du_j. \quad (31)$$

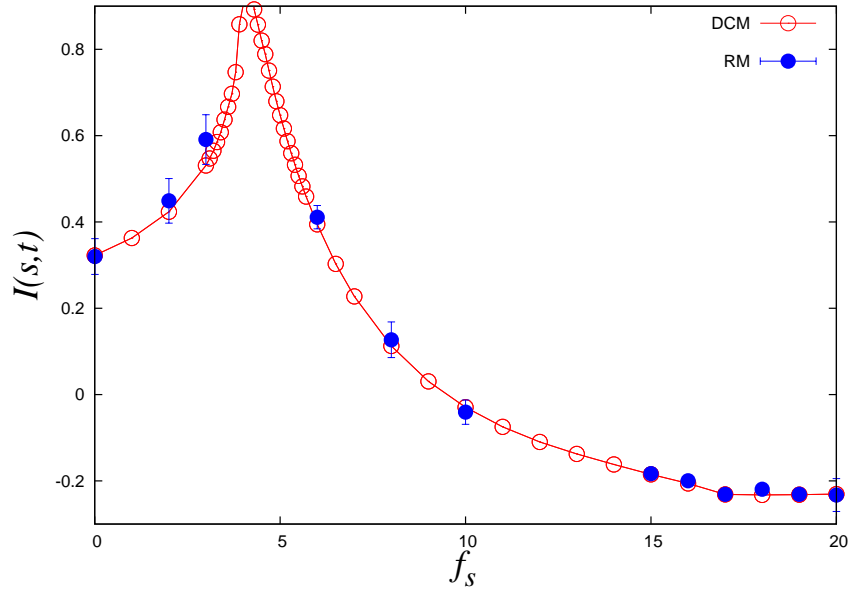


Figure 4: Numerical results of $\Re(I_{non-planar})$ in units of $10^{-12} \text{ GeV}^{-6}$ for $0.0 \leq f_s \leq 20.0$. Values calculated by DCM and those by RM are shown by circles and bullets with error bars, respectively.

In Eqs.(9) and (14), the above expression is integrated over ρ and ξ . Here $\Delta_4 = 0$ can occur in ρ - ξ space, and is regularized numerically by setting the integrand to zero in the vicinity of this anomaly.

The right-hand side is immediately integrated once. Applying the reduction repeatedly to the form in the right-hand side, we see that the original integral is finally replaced by a sum of integrals of functions involving logarithms. Thus the severity of the integrand singularity is reduced, which allows performing the integration even with Monte Carlo routines. Note that this procedure generally creates lengthy expressions. The imaginary part results from the logarithms; let R be a positive number and let $z = -R \pm i\epsilon$, then $\log z = \log(-R \pm i\epsilon) = \log R \pm i\pi$. We refer to this integration method as the *Reduction Method* (RM). We computed the two-loop box integrals by using BASES [47]. The real part of the planar diagram integral in the physical region, shown in [19], is in good agreement with the results by DCM. On the other hand, for the imaginary part, the Monte Carlo integration failed to convergence satisfactorily.

In Fig. 4 we show the real part of the non-planar case obtained by the reduction formulas. Agreement with the results by DCM is poor around the threshold $f_s = 4$ in view of poor convergence of the integration by RM. This may be caused by the numerical regularization in the vicinity of $\Delta_4 = 0$ as mentioned above.

5.2. Consistency check using dispersion relation

The dispersion relation provides a good tool for a consistency check. Based on the observation that $I(s)$ can be regarded as an analytic function in the complex s -plane, the real part and the imaginary part, $\Re(I(s))$ and $\Im(I(s))$, of $I(s)$ satisfy the *dispersion relation*,

$$\Re(I(s)) = \frac{1}{\pi} \text{P} \int_{-\infty}^{+\infty} \frac{\Im(I(s'))}{s - s'} ds', \quad (32)$$

where P denotes principal value integral. Recall that $I(s)$ is real in some region of s and accordingly $\Im(I(s))$ vanishes there. This integral relation, which is the consequence of the analyticity of $I(s)$, implies the real part can be estimated from the imaginary part. DCM computes the real and the imaginary part independently, as they are given by separate integrals. However, the dispersion relation indicates that both parts are not independent. They should be consistent with the relation of Eq. (32).

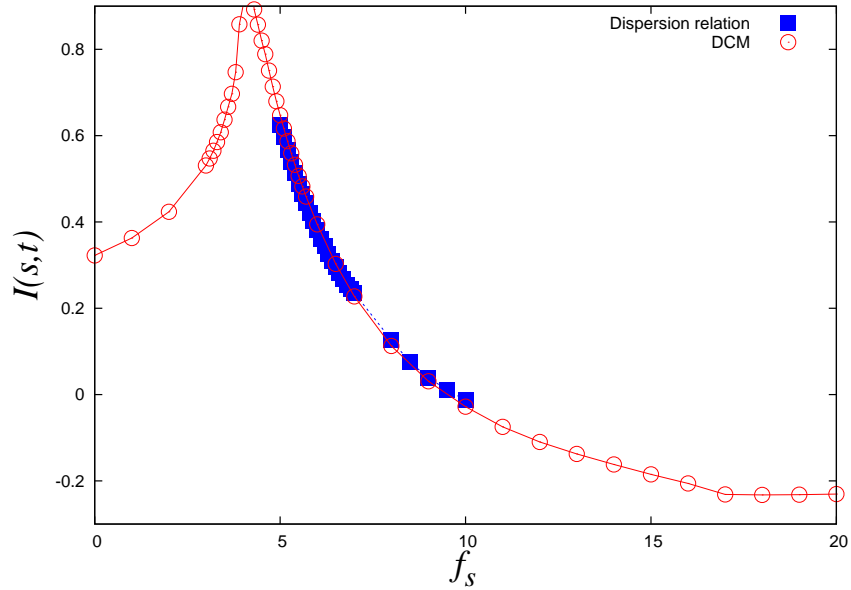


Figure 5: Numerical results of $\Re(I_{non-planar})$ in units of $10^{-12} \text{ GeV}^{-6}$ for $0.0 \leq f_s \leq 20.0$. Values calculated by DCM and those by the dispersion relation are shown by circles and squares, respectively.

In order to show how this relation works we consider the two-loop non-planar box as an example. In this case the integral can be written as

$$\Re(I(s)) = \frac{1}{\pi} \left(\text{P} \int_{-\infty}^{s_0} \frac{\Im(I(s'))}{s - s'} ds' + \text{P} \int_{s_0}^{\infty} \frac{\Im(I(s'))}{s - s'} ds' \right), \quad (33)$$

where $s_0 = 4m^2$ and $s'_0 = -t - M^2 - 4mM$ are the threshold in the s -channel and in the u -channel, respectively, as described in Section 4.2.

For the principal value integral computation we used the trapezoidal rule, assuming that $\Im(I(s)) = 0$ far away from the origin, for $f_s \leq -100.0$ and $f_s \geq 50.0$. Values of $\Re(I(s))$ resulting from this computation are plotted in Fig. 5 for $0.0 \leq f_s \leq 10.0$. The results show good agreement with those by DCM. Thus the relation of Eq. (32) enables a consistency check for the answers produced by DCM.

6. Conclusions

In this paper we calculated the scalar integrals of two-loop planar and non-planar box diagrams involving massive particles. We introduced the *Direct Computation Method* (DCM) for the evaluation. The novel idea in DCM is that the ϵ value in the propagators is treated numerically as a finite number, not as an infinitesimal value. In view of the finite ϵ , the integrand of the loop integral is no longer singular. The integration can be carried out numerically for both the real part and the imaginary part. Consecutive integrations, for each ϵ_l , produce a sequence of integrals $I(\epsilon_l)$, $l = 0, 1, \dots$, which are supplied to the extrapolation procedure. A numerical answer for the loop integral results in the limit as ϵ_l tends to 0.

Since DCM does not impose restrictions on the values of mass parameters, the method is valid when masses are complex [17]. For this case we can put $\epsilon = 0$ where no extrapolation is needed in the same manner as in the non-physical region. This flexibility is remarkable and useful for the calculation of cross-sections where decaying particles are involved.

In order to check our evaluations we compared the results with those obtained by other methods [46], including *Reduction Method* (RM). Comparisons of the results have shown satisfactory agreement. The examination of the

dispersion relation has lead to a consistency check between the real and the imaginary part of the integral. Thus we have established various ways to confirm the results.

Some issues linked with the implementation of parameters, *e.g.*, the choice of ϵ_l values, need to be solved heuristically. Furthermore, in some regions of the kinematical variables, DCM requires very long CPU times to obtain reasonable accuracy. It may be possible to tackle the CPU time problem by utilizing recent developments in computer resources and parallel computing technologies [17, 44, 45]. Throughout this paper we use double precision arithmetic, but quadruple or extended precision may be needed for some mass configurations, including a small fictitious mass λ to regularize infrared divergent integrals [16]. This can be incorporated in dedicated program packages [48, 49].

For a specified high-energy reaction, all the necessary two-loop diagrams can be generated automatically using the GRACE system [4]. The next stage, which involves the automatic generation of amplitudes (*i.e.*, the integrands of loop-integrals), would be manageable in view of the experience we gained in handling tree and one-loop processes [4]. Thus the only component which needs further development for the construction of an automatic computation system for two-loop reactions is a robust loop integral evaluation system.

Concerning the further development of DCM we need to test integrals for various mass configurations different from those in this paper, particularly, infrared divergent integrals by the prescription using a fictitious mass. We also need to examine loop integrals with a non-trivial numerator, and explore a systematic treatment of ultra-violet divergence. From a technical point of view, reducing CPU time and automatic tuning of the integration parameters should be included. After completion of these studies, we expect that DCM will play an important role in constructing automatic computation systems for higher-order corrections.

Acknowledgements

We wish to thank Prof. T.Kaneko for valuable discussions and comments. This work was supported in part by the Grant-in-Aid (No.20340063 and No.23540328) of JSPS and by the CPIS program of Sokendai.

Appendix A. Construction of the functions D and C

For a given diagram, the explicit form of the functions D and C is determined by the following steps [50, 51, 52].

- Step 1.

1. Assign the parameter x_i to the i -th internal line. The parameters $\{x_i\}$ satisfy $\sum_{i=1}^N x_i = 1$.
2. Define L topologically independent loops and label them as $a = 1, \dots, L$. The loop momentum l_a flows through the a -th loop in its own direction.
3. External momenta $p_j, j = 1, \dots, K$ are presumed to enter the diagram inward. Here K is the number of external lines. We let p_j flow through the diagram while respecting the momentum conservation at each vertex. A simple example is where each $p_j, j = 1, \dots, K-1$ flows through the diagram along a continuous path, to reach the vertex where p_K enters. In this case the momentum conservation is trivial as $\sum_{j=1}^K p_j = 0$.
4. Each internal line has its direction and the momentum k_i for the i -th internal line is defined along this direction. It can be expressed by a linear combination of the l_a and p_j as

$$k_i = \sum_{a=1}^L \sigma_a^i l_a + \sum_{j=1}^K \tilde{\sigma}_j^i p_j$$

where

$$\sigma_a^i = \begin{cases} 1 & l_a \text{ flows along the } i\text{-th internal line parallel to its direction} \\ -1 & l_a \text{ flows along the } i\text{-th internal line anti-parallel to its direction} \\ 0 & (\text{otherwise}) \end{cases}$$

and $\tilde{\sigma}_j^i$ can be defined in a similar manner for p_j . We define $p_{ext,i} = \sum_{j=1}^K \tilde{\sigma}_j^i p_j$ for the i -th internal line.

5. It should be noted that, even though the choice of the L -loops, the selection of loop-momenta l_a , and the flow of external momenta are not unique, the final result is the same for any choice.

- Step 2.

We construct an $L \times L$ symmetric matrix A , an L -vector B and a scalar c .

$$A_{ab} = \sum_{i=1}^N \sigma_a^i \sigma_b^i x_i, \quad B_a = \sum_{i=1}^N \sigma_a^i x_i p_{ext,i}, \quad c = \sum_{i=1}^N x_i (p_{ext,i}^2 - m_i^2).$$

- Step 3.

The functions C and D are obtained by

$$C = \det(A), \quad \text{and} \quad D = -\det \begin{pmatrix} A & B \\ B^T & c \end{pmatrix}.$$

D is a homogeneous polynomial of degree $L + 1$, and C is a homogeneous polynomial of degree L in x_i .

Appendix B. Two-loop box diagrams

Following these prescriptions, D and C (Eqs. (7), (8)) for the two-loop planar diagram (Fig. 6(a)) are obtained from

$$\begin{aligned} A_{11} &= x_1 + x_2 + x_3 + x_4, & A_{12} &= A_{21} = -x_4, & A_{22} &= x_4 + x_5 + x_6 + x_7, \\ B_1 &= x_1 p_1 - x_2 p_2, & B_2 &= x_5 p_1 - x_6 p_2 + x_7 (p_1 + p_3), \\ c &= x_1 (p_1^2 - m_1^2) + x_5 (p_1^2 - m_5^2) + x_2 (p_2^2 - m_2^2) + x_6 (p_2^2 - m_6^2) \\ &\quad + x_7 ((p_1 + p_3)^2 - m_7^2) + x_3 (-m_3^2) + x_4 (-m_4^2), \end{aligned}$$

and those (Eqs. (12), (13)) for non-planar diagram (Fig. 6(b)) from

$$\begin{aligned} A_{11} &= x_1 + x_2 + x_3 + x_4 + x_5, & A_{12} &= A_{21} = x_1 + x_2 + x_3, \\ A_{22} &= x_1 + x_2 + x_3 + x_6 + x_7, \\ B_1 &= -(x_1 + x_4) p_3 - x_3 (p_1 + p_3) + x_2 p_4, & B_2 &= (x_2 + x_6) p_4 - x_3 (p_1 + p_3) - x_1 p_3, \\ c &= x_1 (p_3^2 - m_1^2) + x_4 (p_3^2 - m_4^2) + x_2 (p_4^2 - m_3^2) + x_6 (p_4^2 - m_6^2) \\ &\quad + x_3 ((p_1 + p_3)^2 - m_3^2) + x_5 (-m_5^2) + x_7 (-m_7^2). \end{aligned}$$

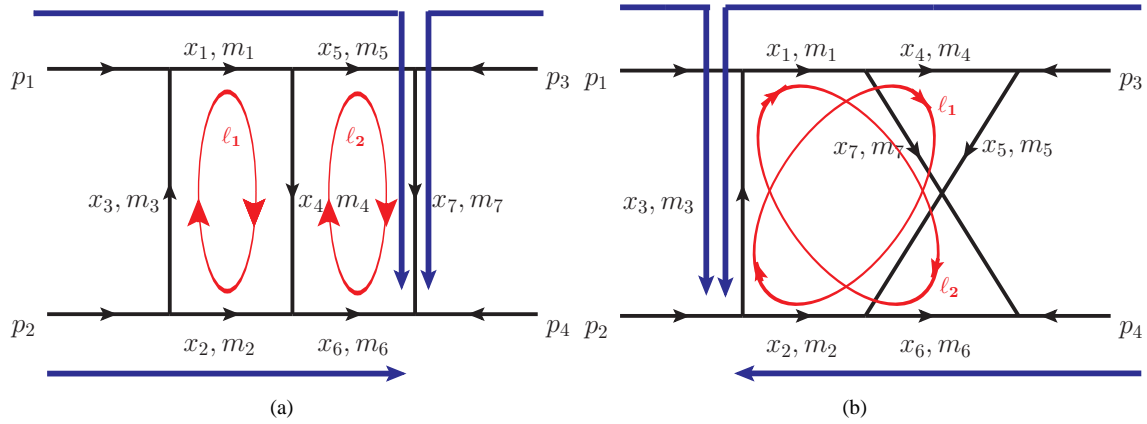


Figure B.6: The quantities in Appendix B are obtained from the configuration shown in the figure for (a) two-loop planar box and (b) two-loop non-planar box. The arrow on each internal line defines its direction (Step 1.4). Red lines and blue lines show the flow of loop momenta (ℓ_a , Step 1.2) and that of external momenta (p_j , Step 1.3), respectively.

References

- [1] G. J. van Oldenborgh and J.A.M. Vermaseren, *New Algorithms for One-Loop Integrals*, Z. Phys. **C46** (1990) 425.
- [2] T.Hahn, *Automatic loop calculations with FeynArts, FormCalc and LoopTools*, Nucl. Phys. Proc. Suppl. **89** (2000) 231, [arXiv:hep-ph/0005029].
- [3] C. Bauer, in Proceedings of *Computer Particle Physics (CPP 2001)*, 27-30 November 2001, Tokyo, in (**KEK Proceedings 2002-11**, Aug 2002 pp.179-185), [MZ-TH/02-04].
Do Hoang Son, Ph.D thesis at the Physics Department, Johannes Gutenberg-Universität Mainz, May 27, 2003.
- [4] G. Bélanger, F. Boudjema, J. Fujimoto, T. Ishikawa, T. Kaneko, K. Kato, Y. Shimizu, *Automatic calculations in high energy physics and GRACE at one-loop*, Phys. Rept. **430** (2006) 117.
- [5] W. T. Giele and G. Zanderighi, *On the Numerical Evaluation of One-Loop Amplitudes: the Gluonic Case*, JHEP **0806** (2008) 038 [arXiv:0805.2152 [hep-ph]].
- [6] G. Bevilacqua, M. Czakon, M.V. Garzelli, A. van Hameren, A. Kardos, C.G. Papadopoulos, R. Pittau, M. Worek, *HELAC-NLO*, [arXiv:1110.1499v1 [hep-ph]].
- [7] V. Hirschi, R. Frederix, S. Frixione, M. V. Garzelli, F. Maltoni and R. Pittau, *Automation of one-loop QCD corrections*, [arXiv:1103.0621 [hep-ph]].
- [8] C. F. Berger, Z. Bern, L. J. Dixon, F. Febres Cordero, D. Forde, H. Ita, D. A. Kosower, D. Maitre, *Automated implementation of on-shell methods for one-loop amplitudes*, Phys. Rev. D **78** (2008) 036003 [arXiv:0803.4180 [hep-ph]].
- [9] G.Cullen, J.-Ph.Guillet, G.Heinrich, T.Kleinschmidt, E.Pilon, T.Reiter, M.Rodgers, *Golem95C: A library for one-loop integrals with complex masses*, [arXiv:1101.5595v1 [hep-ph]].
- [10] G.Cullen, N.Greiner, G.Heinrich, G.Luisoni, P.Mastrolia, G.Ossola, T.Reiter, F.Tramontano, *Automated One-Loop Calculations with GoSam*, [arXiv:1111.2034v1 [hep-ph]].
- [11] E.de Doncker, Y.Shimizu, J.Fujimoto and F.Yuasa, *On a numerical evaluation of loop integrals*, Talk at LoopFest II, May 14-16, 2003. BNL, USA, <http://quark.phy.bnl.gov/loopfest2/program.html>.
- [12] E.de Doncker, Y.Shimizu, J.Fujimoto, F.Yuasa, *Computation of Loop Integrals using Extrapolation*, Comput. Phys. Commun. **159** (2004) 145.
- [13] E.de Doncker, Y.Shimizu, J.Fujimoto, F.Yuasa, K.Kaugars, L.Cucos, J.Van Voorst, *Loop integration results using numerical extrapolation for a non-scalar integral*, Nucl. Instr. Meth. Phys. Res. A **534** (2004) 269.
- [14] E.de Doncker, S.Li, Y.Shimizu, J.Fujimoto, F.Yuasa, *Regularization and Extrapolation Methods for Infrared Divergent Loop Integrals*, Springer Lecture Notes in Computer Science (LNCS) **3514**, (2005) 165.
- [15] E.de Doncker, Y.Shimizu, J.Fujimoto, F.Yuasa, *Numerical Computation of a Non-Planar Two-Loop Vertex Diagram*, Talk at LoopFest V, June 19-21, 2006. SLAC, USA, <http://www-conf.slac.stanford.edu/loopfestv/proc/proceedings.htm>.
- [16] F.Yuasa, E.de Doncker, J.Fujimoto, N.Hamaguchi, T.Ishikawa, Y.Shimizu, *Precise Numerical Results of IR-vertex and box integration with Extrapolation Method*, PoS(ACAT)087.
- [17] F.Yuasa, T.Ishikawa, J.Fujimoto, N.Hamaguchi, E.de Doncker, Y.Shimizu *Numerical Evaluation of Feynman Integrals by a Direct Computation Method*, PoS(ACAT08)122.
- [18] E.de Doncker, J.Fujimoto, N.Hamaguchi, T.Ishikawa, Y.Kurihara, Y.Shimizu, F.Yuasa, *Transformation, reduction and extrapolation techniques for Feynman loop integrals*, Springer Lecture Notes in Computer Science (LNCS) **6017**, (2010) 139.
- [19] E.de Doncker, J.Fujimoto, N.Hamaguchi, T.Ishikawa, Y.Kurihara, Y.Shimizu, F.Yuasa, *Quadpack computation of Feynman loop integrals*, Journal of Computational Science (JoCS) doi:10.1016/j.jocs.2011.06.003 (2011)
- [20] E.de Doncker and F.Yuasa, *Toward Automatic Regularization for Feynman Loop Integrals in Perturbative Quantum Field Theory*, in

- chapter 14 of *Measurement in Quantum Mechanics*, edited by Mohammad Reza Pahlavani, 2012, ISBN 978-953-51-0058-4, <http://www.intechopen.com/books/measurements-in-quantum-mechanics>
- [21] E.de Doncker, F.Yuasa and Y.Kurihara, *Regularization of IR-divergent loop integrals*, proceedings of 14th International Workshop on Advanced Computing and Analysis Techniques in Physics Research, (ACAT 2011), September 5-9, Brunel University, Uxbridge, London, UK, Journal of Physics: Conference Series (JPCS) to be published.
 - [22] K. Kato, E. de Doncker, N. Hamaguchi, T. Ishikawa, T. Koike, Y. Kurihara, Y. Shimizu and F. Yuasa, *Numerical approach to multi-loop integrals*, PoS(QFTHEP2011)029.
 - [23] Y.Oyanagai, T.Kaneko, T.Sasaki, S.Kawabata and Y.Shimizu, *How to Calculate One-Loop Diagrams in Perspectives of Particle Physics*, World Scientific 1989 ISBN 9971-50-589-4, p.369.
 - [24] J.Fujimoto, M.Igarashi, N.Nakazawa Y.Shimizu, K.Tobimatsu, *Radiative Corrections to e^+e^- Reactions in Electroweak Theory*, Prog. Theor. Phys. Suppl. **No.100** (1990) 1.
 - [25] J.Fujimoto, Y.Shimizu, K.Kato and Y.Oyanagi, *Numerical Approach to One-loop Integrals* in Proceedings of Computing in High Energy Physics '91, Universal Academy Press, Inc., Tokyo, Japan 1991, p.407.
 - [26] J.Fujimoto, Y.Shimizu, K.Kato and Y.Oyanagi, *Numerical Approach to One-Loop Integrals*, Prog. Theor. Phys. **Vol.87** (1992) 1233.
 - [27] D. Kreimer, Phys. Lett. **B273** (1991)277.
 - [28] J. Fujimoto, Y. Shimizu, K. Kato and Y. Oyanagi, *Numerical approach to loop integrals*, in *New Computing Techniques in Physics Research II*, World Scientific, 1992, p.625.
 - [29] J.Fujimoto, Y.Shimizu, K.Kato and Y.Oyanagi, *Numerical Approach to Two-loop Integrals*, in Proceedings of VIIth Workshop on High Energy Physics and Quantum Field Theory, Sochi, Russia, Oct 7-14, 1992.
 - [30] J.Fujimoto, Y.Shimizu, K.Kato and T.Kaneko, *Numerical Approach to Two-loop Three point Functions with Masses*, Int. J. Mod. Phys. **C6** (1995)525.
 - [31] O.V.Tarasov, *An algorithm for the small momentum expansion of Feynman diagrams*, in *New Computing Techniques in Physics Research IV*, World Scientific, 1995, p.161.
 - [32] S.Bauberger and M.Bohm, *Simple one-dimensional integral representations for two-loop self-energies: the master diagram*, Nucl. Phys. **B445** (1995) 25.
 - [33] G.Passarino and S.Uccirati, *Algebraic-numerical evaluation of Feynman diagrams: two-loop self-energies*, Nucl. Phys. **B629** (2002) 97.
 - [34] A.Ferrogli, M.Passera, G.Passarino, S.Uccirati, *Two-loop vertices in quantum field theory: infrared convergent scalar configurations*, Nucl. Phys. **B680** (2004) 199.
 - [35] Y.Kurihara and T.Kaneko, *Numerical contour integration for loop integrals*, Comput. Phys. Comm. **174** (2006) 530.
 - [36] C.Anastasiou, S.Beerli, A.Daleo, *Evaluating multi-loop Feynman diagrams with infrared and threshold singularities numerically*, JHEP 0705:071,2007, [arXiv:hep-ph/0703282v2].
 - [37] W.Gong, Z.Nagy, D.E.Soper, *Direct numerical integration of one-loop Feynman diagrams for N-photon amplitudes*, Phys. Rev. **D79** ,033005 (2009), [arXiv:hep-ph/0812.3686].
 - [38] T.Ueda, J.Fujimoto, *New implementation of the sector decomposition in FORM*, PoS(ACAT08)120 and private communication.
 - [39] S.Becker, D.Goetz, C.Reuschle, C.Schwan, S.Weinzierl, *Multiparton NLO corrections by numerical methods*, [arXiv:1112.3521v1 [hep-ph]].
 - [40] R. Piessens, E. de Doncker, C. W. Uebelhuber and D. K. Kahaner, *QUADPACK, A Subroutine Package for Automatic Integration*, Springer Series in Computational Mathematics. Springer-Verlag, 1983.
 - [41] S.Li, E.de Doncker, and K.Kaugars, *On Iterated Numerical Integration*, Springer Lecture Notes in Computer Science (LNCS) **3514**, (2005) 123.
 - [42] D.Shanks, *Non-linear transformations of divergent and slowly convergent sequences*, J. Math. Phys. **34** (1955) 1.
 - [43] P.Wynn, *On a device for calculating the $e_m(S_m)$ transformations*, Mathematical Tables Aids to Computing **10** (1956) 91.
P.Wynn, *On the convergence and stability of the epsilon algorithm*, SIAM J. Numer. Anal. **3** (1966) 91.
 - [44] E.de Doncker, *Parallel Iterated Multivariate Integration*, Talk at the International Conference on Computational and Applied Mathematics (ICIAM), July 18-22, 2011. Vancouver, Canada.
 - [45] E.de Doncker and F.Yuasa, *Parallel Computation of Feynman Loop Integrals*, proceedings of Conference on Computational Physics (CCP 2011), October 30-November 3, Oakridge National Laboratory (ORNL), Gatlinburg, Tennessee, Journal of Physics: Conference Series (JPCS) to be published.
 - [46] S.Laporta, *High-precision calculation of multi-loop Feynman integrals by difference equations*, Int. J. Mod. Phys. **A15** (2000)5087.
 - [47] S.Kawabata, *A new version of the multi-dimensional integration and event generation package BASES/SPRING* Comput. Phys. Comm. **88** (1995) 309.
 - [48] J. Fujimoto, N.Hamaguchi, T. Ishikawa, T.Kaneko, H. Morita, D. Perret-Gallix, A. Tokura, Y.Shimizu, *Numerical precision control and GRACE*, Nucl. Instr. and Meth. **A559** (2006) 269.
 - [49] H.Fujiwara, <http://www-an.acs.i.kyoto-u.ac.jp/~fujiwara/exflib>
 - [50] G.Tiktopoulos, *High-Energy Behavior of Feynman Amplitudes*, Phys. Rev **Vol 131** (1963) 480.
 - [51] R.J.Eden, P.V.Landshoff, D.I.Olive, J.C.Polkinghorne, *The Analytic S-Matrix*, Cambridge University Press, Cambridge, 1966.
 - [52] N.Nakanishi, *Graph Theory and Feynman Integrals*, Gordon and Breach, New York, 1971.